Wireless Power Transfer System with Constant Voltage/Constant Current Output Performance

Xingchen Yang[1,*], Jun Tong[2]

[1]College of Coal and Chemical Industry, Shaanxi Energy Institute, Xianyang 712000, China
[2]School of Electrical and Control Engineering, Xi'an University of Science and Technology, Xi'an 710054, China

[*]Corresponding author: yanghu1230@yeah.net

ABSTRACT Aiming at the problem of unstable output voltage and output current caused by load fluctuation, this paper starts from the perspective of system topology and control strategy for analysis. First, the output characteristics of LCL-S (inductor-capacitor-inductor and series), LCL-P (inductor-capacitor-inductor and parallel), LCL-LCL (inductor-capacitor-inductor and inductor-capacitor-inductor), and LCL-LCC (inductor-capacitor-inductor and inductor-capacitor-capacitor) compensation topologies are analyzed. Combining the advantages of LCL-S and LCL-LCL compensation topology output characteristics, an LCL-LCL/S compensation topology is constructed, and its topology is optimized. Then the influence of parasitic resistance on the output characteristics of LCL-LCL/S compensation topology is derived. A control strategy of primary side regulation is proposed to address the issue of unstable output voltage and current caused by parasitic resistance in the system under variable loads. This method can effectively improve the stability of the output voltage and output current of the wireless power transfer system in the LCL-LCL/S compensation topology under load fluctuations. Finally, a set of experimental prototypes is built to verify the correctness of the theoretical analysis.

INDEX TERMS Wireless power transfer; constant voltage output; constant current output; primary side regulation

I. INTRODUCTION

Radio energy transmission technology has been widely used in smartphones [1-2], electronic healthcare [3-5], electric vehicles [6-7], and AUVs [8] because of its advantages of high safety, contactless sparks, flexible power supply, and strong environmental adaptability [9-11]. However, how to use wireless power transfer technology to provide stable voltage and current guarantee for electrical equipment with a wide load variation range has become an urgent problem in this field.

To solve the above problem, a multi-winding wireless charging system was proposed to realize constant voltage and constant current charging in a wide load variation range [12]. A four-coil structure wireless power transfer system based on dual-frequency switching method was proposed to charge the load with constant voltage and constant current at two fixed zero-phase points [13]. Gong et al. [14] adopted LCC-S/LCC compensation network to achieve constant voltage and constant current output of the system by switching the compensation network at the receiving end. Liu et al. [15] analyzed the circuit models of LCC and LCL transformation networks, and concluded that, when the parameters of network components meet certain conditions, they can achieve constant voltage and constant current output within a certain load range. Zhou et al. [16] used LCC-LCC compensation network to realize the constant voltage and constant current output of wireless power transfer system, so as to effectively reduce the current harmonics by switching the resonance point of the system, and improve the transmission efficiency and anti-offset ability of the system. Based on LC-CLC resonant network, the realization conditions of constant current/constant voltage output characteristics and the calculation methods of constant current frequency and constant voltage frequency are derived, and finally the correctness and validity of the theory were verified by simulation and experiment [17]. Based on LCC/S resonant network, a wireless power transfer system with continuous switching process, low switching voltage stress, zero voltage opening in full load range, and constant current/constant voltage output characteristics was proposed [18]. Aiming at the output voltage fluctuation when the coupling mechanism was offset, an anti-offset method based on constant voltage output interval tracking was proposed to improve the ability of dynamic regulation of system output voltage [19]. Based on multiple relay coils of a wireless power transfer system, the constant current/constant voltage output of the system was realized by controlling the operating frequency of the system [20].

First, the output characteristics of LCL-S, LCL-P, LCL-LCL, and LCL-LCC compensation topologies are analyzed. Then, combined with the advantages of LCL-S and LCL-LCL compensation topology output characteristics, a circuit model of LCL-LCL/S hybrid compensation topology is established. The influence of parasitic resistance on the constant voltage and constant current output characteristics of LCL-LCL/S compensation topology is analyzed in detail. Aiming at the problem of load fluctuation leading to the unstable output voltage and current of LCL-LCL/S compensation system, a regulation strategy of the front DC/DC converter is proposed. Finally, a set of experimental prototypes is built to verify the correctness of the theoretical analysis. This design method is simple and reliable, and has certain guiding significance for the wireless power transfer technology to provide stable voltage and current guarantee for electrical equipment with a wide load variation range.

II. MATERIALS AND METHODS

The compensation topologies based on LCL resonant circuits include LCL-S type, LCL-P type, LCL-LCL type and LCL-LCC type.Fig.1 shows the schematics of the four compensation topologies based on LCL resonant circuits.

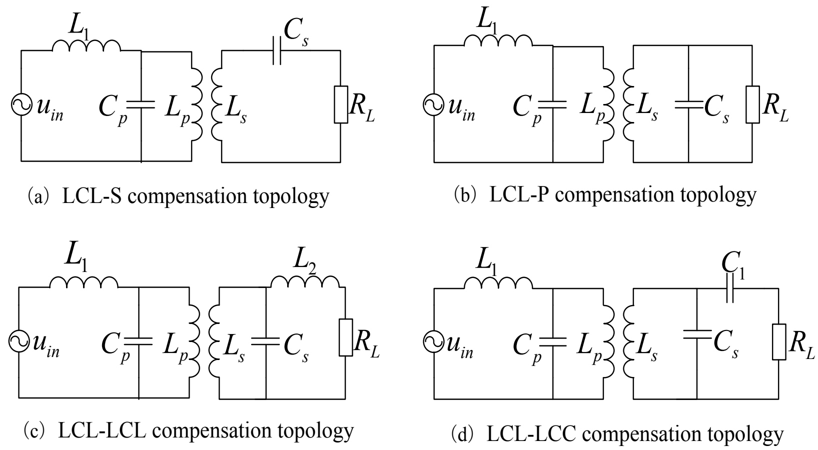

FIGURE 1. Four compensation topologies based on LCL resonant circuit

The LCL-S compensation topology is taken as an example to analyze its output characteristics. Fig. 2 shows the schematic of LCL-S compensation topology.

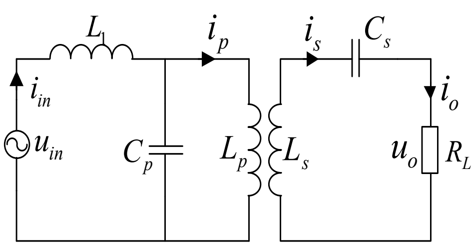

FIGURE 2. LCL-S compensation topology

where, u_{in} is the high frequency AC power supply; i_{in} is the power supply current; i_p is the primary current; L_1, C_p, and L_p constitute the primary LCL resonant circuit together; L_s and C_s form a secondary side series resonant circuit together; R_L is the equivalent load; u_o and i_o are the output voltage and current, respectively; M is the mutual inductance value of the primary and secondary sides; ω is the angular frequency of the high-frequency AC power supply, ω=2πf. According to the circuit principle, the equivalent impedance Z_s of the secondary side can be obtained as follows:

$$Z_s = R_L + j\omega L_s + \frac{1}{j\omega C_s} \tag{1}$$

The reflected impedance Z_r formed by the reflection of the secondary side impedance onto the original side is as follows:

$$Z_r = \frac{\omega^2 M^2}{R_L + \dfrac{1}{j\omega C_s} + j\omega L_s} \tag{2}$$

Then, the total impedance Z_{in} of the primary-side input is as follows:

$$Z_{in} = j\omega L_1 + \frac{1}{j\omega C_p + \dfrac{1}{j\omega L_p + Z_r}} \tag{3}$$

The supply current $\dot{I}_{in}$ is as follows:

$$\dot{I}_{in} = \frac{\dot{U}_{in}}{j\omega L_1 + \cfrac{1}{\cfrac{1}{j\omega L_p + Z_r} + j\omega C_p}} \tag{4}$$

The primary current I_P is as follows:

$$\dot{I}_p = \frac{\dot{U}_{in}}{Z_r(1-\omega^2 L_1 C_p) + j\omega(L_1 + L_p) - j\omega^3 L_1 L_p C_p} \tag{5}$$

When $\omega = 1/\sqrt{L_P C_P} = 1/\sqrt{L_s C_s}$, $L_1 = L_P$, the primary current $\dot{I}_p$ can be simplified as:

$$\dot{I}_p = \frac{\dot{U}_{in}}{j\omega L_p} \tag{6}$$

The output voltage and current can be derived as:

$$\dot{U}_o = \dot{U}_{in}\frac{M}{L_p} \tag{7}$$

$$\dot{I}_o = \frac{\dot{U}_o}{R_L} = \frac{\dot{U}_{in} M}{L_p R_L} \tag{8}$$

It can be seen from Eq. (7), the output voltage value of the LCL-S compensation topology is only related to the inherent parameters of the system and the value of the input voltage U_{in}, and not to the value of the load resistance R_L. The LCL-S compensation topology thus has constant voltage output characteristics. Moreover, when the system operates at the natural frequency of the secondary side, the equivalent impedance Z_s of the secondary side of the LCL-S t compensation topology is purely resistive, and its reflected impedance Z_r is also pure resistive. The reflected impedance z_r does not affect the operating frequency of the system.

In the same way, the output characteristics of LCL-P, LCL-LCL and LCL-LCC compensation topology can be obtained separately, and the specific analysis process will not be repeated. The results of the analysis are shown in Table I. Table I shows the output characteristics of LCL-S, LCL-P, LCL-LCL, and LCL-LCC compensation topologies under specific parameter configurations.

TABLE I. Output characteristics of four compensation topologies

Topology structure	Whether it has constant voltage output characteristics	Whether Z_r is purely resistive	Whether it has constant current output characteristics	Whether Z_r is purely resistive
LCL-S	√	√	×	×
LCL-P	×	×	√	×
LCL-LCL	√	×	√	√
LCL-LCC	√	×	√	×

It can be seen from Table I that, the LCL-S compensation topology has optimal constant voltage output performance, and the LCL-LCL compensation topology has optimal constant current output performance. Moreover, under these conditions, its reflected impedance is purely resistive. Combining the advantages of LCL-S and LCL-LCL compensation topology output characteristics, a hybrid compensation topology with constant voltage and constant current output performance - LCL-LCL/S compensation topology is formed.

Fig. 3(a) shows the schematic of the LCL-LCL/S compensation topology. LCL-LCL/S compensation topology consists of two parts: when the system requires constant voltage output, LCL-S compensation topology can be selected; when the system requires a constant current output, it can be switched to an LCL-LCL compensation topology. To reduce the design cost and the volume of the device, S1, S2, and S3 can be switched on and off to achieve the purpose of switching the output state of the system. As shown in Fig. 3(b), when the switches S1 and S3 are closed and S2 is off, the system is in a constant current output state; when the switch S2 is closed, S1 and S3 are off, the system is in a constant voltage output state.

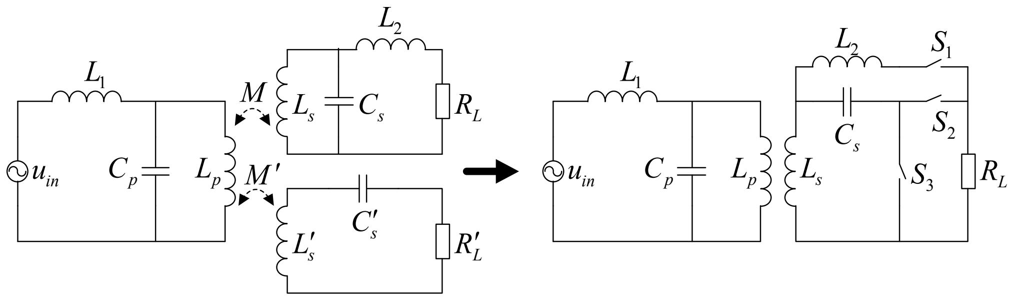

（a） LCL-LCL/S compensation topology （b） Simplified diagram

FIGURE 3. Schematic and simplified diagram of the LCL-LCL/Se compensation topology

In a real-world circuit, there are many parameters that affect the output performance of the LCL-LCL/S compensation topology. Among them, parasitic resistance has the greatest influence. Fig. 4 shows the schematic of an LCL-S compensation topology considering parasitic resistance.

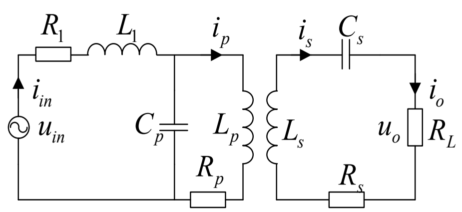

FIGURE 4. The LCL-S compensation topology considering parasitic resistance

where, R_1, R_p, and R_s are the parasitic resistance of the inductance L_1, L_p, and L respectively. According to the circuit principle, it can be deduced that the LCL-S compensation topology works under constant voltage output conditions, and its output voltage and output current are:

$$\begin{cases} \dot{U}_o = \dfrac{R_L}{R_L+R_s} \bullet \dfrac{\dot{U}_{in}M}{L_p + C_pR_1\left(R_p + \dfrac{\omega^2M^2}{R_L+R_s}\right)} \\ \dot{I}_o = \dfrac{1}{R_L+R_s} \bullet \dfrac{\dot{U}_{in}M}{L_p + C_pR_1\left(R_p + \dfrac{\omega^2M^2}{R_L+R_s}\right)} \end{cases} \tag{9}$$

Fig. 5 shows the schematic of an LCL-LCL compensation topology considering parasitic resistance.

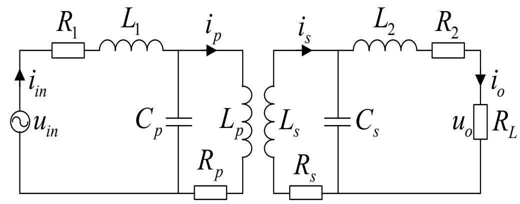

FIGURE 5. LCL-LCL compensation topology considering parasitic resistance

Similarly, based on circuit principles, it can be inferred that the LCL-LCL compensation topology operates under constant current output conditions, and its output voltage and current are as follows:

$$\begin{cases} \dot{U}_o = \dfrac{M}{L_2 + C_sR_sR_L} \bullet \dfrac{\dot{U}_{in}R_L}{j\omega L_p + j\omega C_pR_1Z_x} \\ \dot{I}_o = \dfrac{M}{L_2 + C_sR_sR_L} \bullet \dfrac{\dot{U}_{in}}{j\omega L_p + j\omega C_pR_1Z_x} \end{cases} \tag{10}$$

where, Z_x is as follows:

$$Z_x = R_p + \frac{\omega^2M^2}{R_s + \dfrac{L_2}{C_s\left(R_2+R_L\right)}} \tag{11}$$

To verify the correctness of the theoretical analysis, the LCL-S compensation topology and LCL-LCL compensation topology are constructed according to Fig. 4 and Fig. 5 with MATLAB simulation software, and the simulation parameters are shown in Table II.

TABLE II. Simulation parameters

Parameters	Topology structure		Parameters	Topology structure	
	LCL-S	LCL-LCL		LCL-S	LCL-LCL
f	25KHz	25KHz	C_p	$9e^{-7}$F	$9e^{-7}$F
u_{in}	27V	27V	C_s	$9e^{-7}$F	$9e^{-7}$F
L_1	$45e^{-6}$H	$45e^{-6}$H	R_1	0.5Ω	0.5Ω

L_p	$45e^{-6}$H	$45e^{-6}$H	R_p	0.5Ω	0.5Ω
L_2	/	$45e^{-6}$H	R_2	/	0.5Ω
L_s	$45e^{-6}$H	$45e^{-6}$H	R_s	0.5Ω	0.5Ω
M	$20e^{-6}$H	$20e^{-6}$H			

The simulation results are shown in Table III and Table IV.

TABLE III. Comparison of theoretical and simulation values of LCL-S compensation output voltage

Resistance /Ω	10	20	30	40	50	60	70	80	Conversion rate%
Simulation value /V	11.28	11.63	11.75	11.81	11.85	11.88	11.89	11.91	5.6%
Theoretical value /V	11.27	11.59	11.71	11.77	11.80	11.82	11.84	11.85	5.1%

TABLE IV. Comparison between the theoretical value of LCL-LCL compensation output current and the simulation value

Resistance/Ω	10	20	30	40	50	60	70	80	Conversion rate%
Simulation value/A	1.504	1.359	1.24	1.139	1.054	0.981	0.917	0.861	42.8%
Theoretical value/A	1.507	1.355	1.228	1.119	1.026	0.945	0.874	0.812	46.1%

Similarly, the equivalent series resistance (ESR) in a capacitor can also affect the output of the system. Based on Table II, the equivalent series resistance of C_p and C_s is set to 0.3 Ω (the equivalent series resistance of capacitors varies at different frequencies and voltages). Using MATLAB simulation software for simulation, the simulation results are shown in Tables V and VI.

TABLE V. Simulation value of LCL-S compensation output voltage considering ESR

Resistance/Ω	10	20	30	40	50	60	70	80	Conversion rate%
Simulation value/V	10.83	11.32	11.50	11.59	11.65	11.68	11.71	11.73	8.3%

TABLE VI. Simulation values of LCL-LCL compensation output current considering ESR

Resistance /Ω	10	20	30	40	50	60	70	80	Conversion rate%
Simulation values/A	1.391	1.201	1.056	0.943	0.851	0.776	0.713	0.660	52.6%

Based on the above simulation results, it can be seen that parasitic resistance has a relatively small impact on the constant voltage output characteristics of the LCL-S compensation topology, but has a significant impact on the constant current output characteristics of the LCL-LCL compensation topology.

To provide high-quality power guarantee for electrical equipment with a wide load variation range, it can be seen from Eqs. (9) and (10) that the output voltage value of LCL-S compensation topology and the output current value of LCL-LCLs compensation topology are related to the value of the input voltage u_{in}. The output voltage and output current of the entire system can be regulated by adjusting the value of the input voltage u_{in}. The basic idea is shown in Fig. 6, and the overall design scheme of the system is shown in Fig. 7.

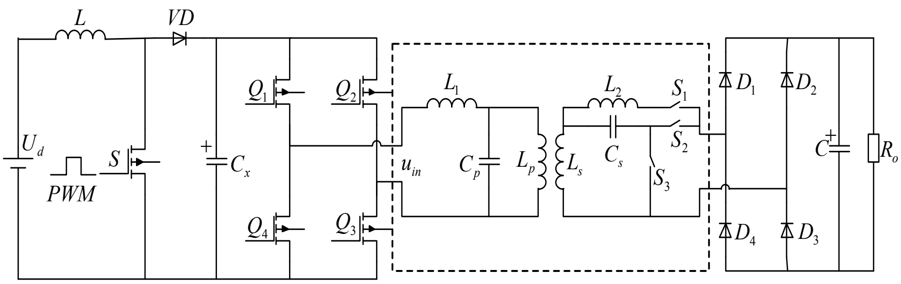

FIGURE 6. Schematic diagram of dynamic adjustment of system output voltage and current

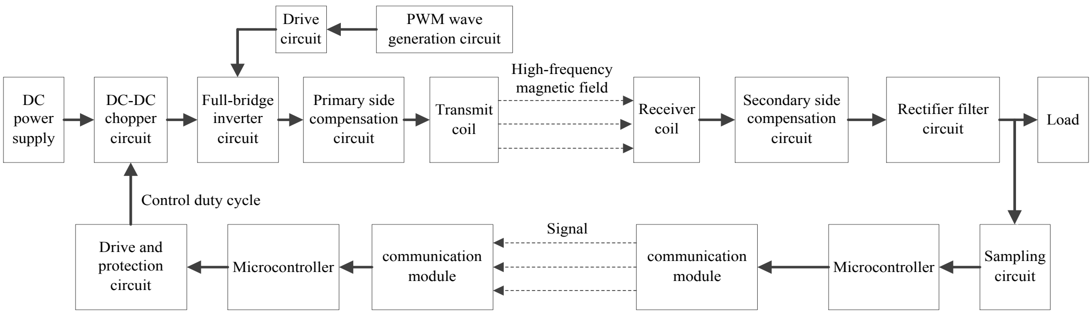

FIGURE 7. Schematic diagram of the overall design of the system

Its basic working principle: the sampling circuit collects the voltage and current information at the load end and transmits the collected information to the microprocessor. Then the microprocessor compares the acquired value with the expected value. When the error between the two is greater than the maximum error limit value, the secondary side microprocessor issues instructions to the primary side microprocessor. The primary side microprocessor regulates the duty cycle of the DC/DC converter to achieve the purpose of adjusting the system output.

III. RESULTS AND ANALYSIS

To verify the correctness of the theoretical analysis, an experimental platform for LCL-LCL/S compensation topology with a front connected Boost converter is built, as shown in Fig. 8. The experimental parameters are a coil pitch of 30mm, an input voltage of U_d=24V, a system operating frequency of f=25KHz, and the inductance of L_1=45.6μH, L_2=46.1 μH, L_p=45.1μH, and L_s=44.7μH. Among them, the parasitic resistances on the inductance are R_1=116mΩ, R_2=128mΩ, R_p=301mΩ, and R_s=293mΩ respectively; the system resonant capacitor is C_p=C_s=900nF, and the variation range of load resistance is 10-40Ω.

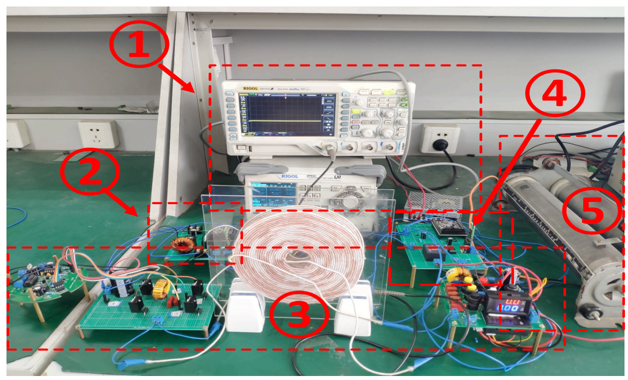

FIGURE 8. Experimental prototype testing platform

This experimental platform mainly consists of 5 parts, corresponding to the labels ① to ⑤ in Fig. 8. Label ① includes a power supply and an oscilloscope, wherein the oscilloscope is mainly used to monitor the drive signal of the pre-amp boost converter to verify that the primary-side minimum system will provide the pre-boost converter with different duty cycle driving signals with the change of load. Label ② includes a primary-side closed-loop circuit and a pre-boost converter. Label ③ is the main circuit of the system, which is composed of a full-bridge inverter circuit, a driving circuit of a full-bridge inverter circuit, an LCL-LCL/S compensation topology circuit, a rectifier filter circuit, and a digital voltage and ammeter. Among them, the digital voltage and current meter is mainly used to monitor the changes of the output voltage value and current value of the system. Label ④ is the secondary side closed-loop circuit, and label ⑤ is the system load.

The experimental results are shown in Figs. 9 and 10.

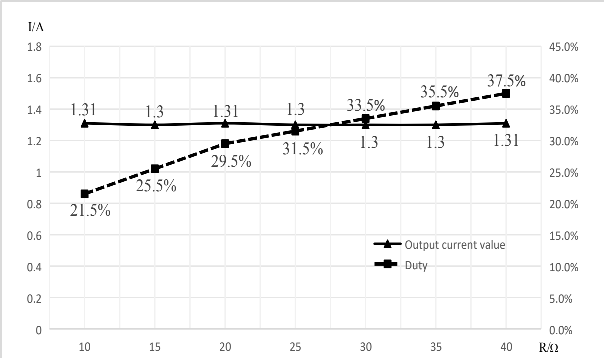

FIGURE 9. Changes in system output current values

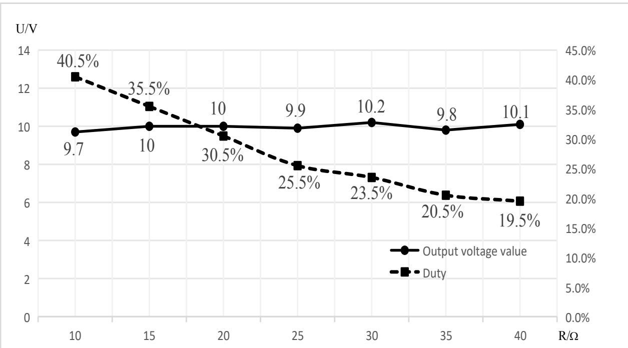

FIGURE 10. Changes in system output voltage values

Fig. 9 shows the diagram of the change of system output current value. It can be seen that as the load resistance increases, the output current value of the system is basically stable at about 1.3A, but the duty cycle of the Boost converter has increased from 21.5% to 37.5%. Fig. 10 shows the change of the output voltage value of the system. It can be seen that with the continuous increase of load resistance, the output voltage value of the system is basically stable at about 10V, but the duty cycle of the Boost converter has decreased from 40.5% to 19.5%. Consequently, adjusting the value of the input voltage u_{in} can effectively improve the output performance of the LCL-LCL/S compensation system.

IV. CONCLUSIONS

This article proposes a control method for dynamically adjusting the output voltage and current of the system to provide stable voltage and current protection for electrical equipment with a wide range of load changes. Through theoretical analysis and experimental verification, the following conclusions are obtained:

(1) LCL-S, LCL-LCL and LCL-LCC compensation topology all have constant voltage output characteristics, and only LCL-S compensation topology has pure resistive impedance under constant voltage output.

(2) LCL-P, LCL-LCL and LCL-LCC compensation topology all have constant current output characteristics, and only LCL-LCL compensation topology has pure resistive impedance under constant current output.

(3) Due to the influence of parasitic resistance, when the load resistance R_L changes, the LCL-S compensation topology will lose the constant voltage output characteristics; the LCL-LCL compensation topology will lose the constant current output characteristic.

(4) Through adjusting the value of the input voltage u_{in}, the output voltage and output current of the entire system can be controlled. Therefore, the stability of the output voltage and output current of the wireless power transfer system of the LCL-LCL/S type compensation topology can be improved by adjusting the duty cycle of the preceding DC/DC converter.

ACKNOWLEDGEMENT

The work was supported by the National Natural Science Foundation of China (51307137); the Project Supported by Natural Science Basic Research Plan in Shaanxi Province of China (Program No. 2018JZ5014); Coal Mine Intelligent Machinery Equipment Research and Innovation Team of Shaanxi Energy Vocational and Technical College (2021KYTD04); 2022 Key Research Projects in Natural Science and Technology at the School Level of Shaanxi Energy Vocational and Technical College: Research and Design of Wireless Charging Device for Mining Inspection Robot (2022KY04KJZ).

REFERENCES

[1] M. R. Gholipour, M. Saradarzadeh, S. Farhangi, "Wireless power transfer pulse charging of lithium-ion battery", *Journal of Energy Storage*, vol. 72, no. Part B, pp. 108402, 2023. https://doi.org/10.1016/j.est.2023.108402

[2] N. Ramsaroop, O. O. Olugbara, "Wireless Power Transfer Using Harvested Radio Frequency Energy with Magnetic Resonance Coupling to Charge Mobile Device Batteries", *Applied Sciences*, vol. 11, no. 16, pp. 7707, 2021. https://doi.org/10.3390/app11167707

[3] X. L. Chang, P. S. Chee, E. H. Lim, "Compact conformal tattoo-polymer antenna for on-body wireless power transfer", *Scientific Reports*, vol. 13, pp. 9678, 2023. https://doi.org/10.1038/s41598-023-36335-6

[4] E. S. Dyachkova, E. A. Mindubaev, A. A. Danilov, "Study of the Power Characteristics and Safety of a Wireless Power Transfer System for Power Supplies for Medical Equipment in Operating Rooms", *Biomedical Engineering*, vol. 56, no. 3, pp. 204-207, 2022. https://doi.org/10.1007/s10527-022-10198-z

[5] D. McEneaney, O. Escalona, A. Bosnjak, M. Karim, P. Crawford, J. McLaughlin, "A Novel Wireless Power Transmission System for Left Ventricular Assist Devices", *Journal of Heart and Lung Transplantation*, vol. 42, no. 4, pp. S183, 2023. https://doi.org/10.1016/j.healun.2023.02.1690

[6] W. Liu, C. Hu, L. Xiang, "A Multimodal Modulation Scheme for Electric Vehicles' Wireless Power Transfer Systems, Based on Secondary Impedance", *Electronics*, vol. 11, no. 19, pp. 3055, 2022. https://doi.org/10.3390/electronics11193055

[7] I. Bentalhik, A. Lassioui, H. EL Fadil, T. Bouanou, A. Rachid, Z. EL Idrissi, A. M. Hamed, Analysis, "Design and Realization of a Wireless Power Transfer Charger for Electric Vehicles: Theoretical Approach and Experimental Results", *World Electric Vehicle Journal*, vol. 13, no. 7, pp. 121, 2022.

https://doi.org/10.3390/wevj13070121
[8] K. Qiao, E. Rong, P. Sun, X. Zhang, J. Sun, “Design of LCC-P Constant Current Topology Parameters for AUV Wireless Power Transfer”, *Energies*, vol. 15, no. 14, pp. 5249, 2022.https://doi.org/10.3390/en15145249
[9] K. Detka, K. Górecki, “Wireless Power Transfer—A Review”, *Energies*, vol. 15, no. 19, pp. 7236, 2022. https://doi.org/10.3390/en15197236
[10] M. T. Tran, S. Thekkan, H. Polat, D. D. Tran, M. El Baghdadi, O. Hegazy, “Inductive Wireless Power Transfer Systems for Low-Voltage and High-Current Electric Mobility Applications: Review and Design Example”, *Energies*, vol. 16, no. 7, pp. 2953, 2023. https://doi.org/10.3390/en16072953
[11] Y. Yamada, S. Hasegawa, T. Imura, Y. Hori, “Coil Design Method Considering Power, Efficiency, and Magnetic Field Strength of Coreless Coils Using Numerical Analysis in Wireless Power Transfer”, *IEEJ Transactions on Electrical and Electronic Engineering*, vol. 18, no. 8, pp. 1360-1370, 2023. https://doi.org/10.1002/tee.23851
[12] Z. Shen, H. Zhou, H. Tang, X. Mao, Y. Zhang, "Reconfigurable topology of electric vehicle wireless power transfer system to achieve constant-current and constant-voltage charging based on multiple windings”, *Energy Reports*, vol. 9, no. S10, pp. 1220-1226, 2023. https://doi.org/10.1016/j.egyr.2023.05.084
[13] L. Yang, X. Yu, Y. Shi, M. Wang, “A four-coil structure wireless power transfer system with constant current and constant voltage charging: Analysis, design, and experiment”, *International Journal of Circuit Theory and Applications*, vol. 51, no. 1, pp. 32-46, 2023. https://doi.org/10.1002/cta.3437
[14] W. Gong, J. Xiao, S. Han, X. Wu, N. Wu, S. Chen, "Research on robot wireless charging system based on constant-voltage and constant-current mode switching”, *Energy Reports*, vol. 8, no. S4, pp. 940-948, 2022. https://doi.org/10.1016/j.egyr.2022.02.025
[15] W. Liu, L. Lin, M. Tian, C. Xu, W. Zhang, “Research on output characteristics of wireless power transmission power source based on transforming network”, *The Journal of Engineering*, vol. 2019, no. 16, pp. 2890-2892, 2019. https://doi.org/10.1049/joe.2018.8916
[16] Y. Zhou, M. Qiu, Q. Wang, Z. Ma, H. Sun, X. Zhang, “Research on Double LCC Compensation Network for Multi-Resonant Point Switching in Underwater Wireless Power Transfer System”, *Electronics*, vol. 12, no. 13, pp. 2798, 2023. https://doi.org/10.3390/electronics12132798
[17] Y.G. Su, Z.Q. Yan, H.S. Hu, Y. Sun, Z. Liu, S.B.Y. Liu, “Electric-Field Coupled Power Transfer System with Constant Current / Constant Voltage Output Characteristics Based on Frequency Switching”, *Proceedings of the CSEE*, pp. 1-13, 2023. DOI:10.13334/j.0258-8013.pcsee.223014
[18] Y.S. Yao, M. Zeng, G. Li, Y.J. Wang, “Switching method from constant current mode to constant voltage mode for wireless power transfer system”, *Electric Machines and Control*, vol. 27, no. 06, pp. 8-17, 2023. DOI:10.15938/j.emc.2023.06.002
[19] W.C. Huang, X.Y. Jiang, Y.F. Chang, H.D. Tan, S.H. Zhu, “Anti-offset method for WPT systems based on constant voltage output in-terval tracking”, *Journal of Power Supply*, pp. 1-13, 2023. http://kns.cnki.net/kcms/detail/12.1420.TM.20230112.1722.002.html
[20] Y.H. Chen, Y.Y. Li, B. Yang, Y. Chen, R.K. Mai, “Constant-current/Constant-voltage Output Method for Wireless Power Transfer System Based on Multi-relay Coil Structure”, *Automation of Electric Power Systems*, vol. 46, no. 20, pp. 147-154, 2022.